

DEPARTMENT OF CHEMISTRY & BIOCHEMISTRY
COLLEGE OF SCIENCES
OLD DOMINION UNIVERSITY
NORFOLK, VIRGINIA 23529

191210
11 34
103383

P. 24

**Ab Initio Atomic Recombination Reaction
Energetics on Model Heat Shield Surfaces**

By

Fredrick Senese, Graduate Research Assistant

and

Robert Ake, Principal Investigator

Ny3-12577

Unclas

63/34 0128332

Final Report
For the period ended August 31, 1992

Prepared for
National Aeronautics and Space Administration
Langley Research Center
Hampton, Virginia 23665

Under
Research Grant NCC1-147
Dr. Donald H. Phillips, Technical Monitor
IRD-Nondestructive Evaluation Sciences Branch

Submitted by the
Old Dominion University Research Foundation
P.O. Box 6369
Norfolk, Virginia 23508-0369

(NASA-CR-191210) AB INITIO ATOMIC
RECOMBINATION REACTION ENERGETICS
ON MODEL HEAT SHIELD SURFACES FINAL
Report, period ending 31 Aug. 1992
(Old Dominion Univ.) 24 p

480341

October 1992



Final Report for Cooperative Agreement Titled
**Ab Initio Atomic Recombination Reaction Energetics
On Model Heat Shield Surfaces**

Fredrick Senese

Contract NCCI147

Task Monitor: Donald H. Phillips

Characterization of the interaction between dissociated air species and thermal protection surfaces is prerequisite for theoretical prediction of surface catalytic phenomena under re-entry conditions. Frozen orbital methodology and software necessary for the ab-initio quantum mechanical calculation of accurate gas-surface interaction potentials has been developed at LaRC under the current contract. The codes compute energies, properties and wavefunctions for large, spatially extended systems using a bootstrap frozen orbital approach.

The codes were applied to several small linear crystalline test systems. Energy shifts caused by variation in the structure of central defect sites are accurately predicted when the bulk-local site interaction was small. In other instances (more representative of those encountered around recombination sites) observed discrepancies with all electron results are due to:

1. Basis set superposition errors (the bulk basis set is inaccessible to the variational treatment and therefore the model results are not subject to spurious lowering of the energy due to superposition of the free and frozen bases)
2. Omission of bonding effects at the boundary in the absence of basis boundary transformations. These errors can be alleviated by increasing the size of the local site and/or by using boundary transformations to efficiently repartition the basis.
3. First order bulk polarization errors. When the defect field is very strong, bulk orbitals can be correctly polarized by self-consistently optimizing them in the defect field.
4. Second order dispersion and charge transfer errors. These errors can be minimized by increasing the size of the local site.

Boundary bonding and bulk polarization effects had the most serious impact on accuracy of the model gas-surface potentials. Further methodological work will be directed towards an improved treatment of boundary effects and towards minimizing the bulk polarization error by means of parallel heterogenous solid calculations.

An application and thorough test of the method involves prediction of the effects of hydration on the electronic structure of the nitrate ion by freezing the description of the second solvation shell. Initial studies are described in the attached paper "Ab Initio Studies of Nitrate Ion Hydration Complexes". The self-consistent field method with accurate basis sets has been applied to compute completely optimized equilibrium geometries, vibrational frequencies, thermochemical parameters, and stable site labilities of complexes involving 1, 2, and 3 waters. This study will be submitted to the Journal of Chemical Physics.

Ab Initio Studies of Nitrate Ion Hydration Complexes

Frederick Senese¹

*Old Dominion University Research Foundation, P. O. Box 6369, 800 W.
46th St., Norfolk VA 23508*

Donald H. Phillips

Mail Stop 231, NASA-Langley Research Center, Hampton, VA 23665

Abstract

Ab initio quantum mechanical calculations on small hydration complexes involving the nitrate anion are reported. The self-consistent field method with accurate basis sets has been applied to compute completely optimized equilibrium geometries, vibrational frequencies, thermochemical parameters, and stable site labilities of complexes involving 1, 2, and 3 waters. The most stable geometries in the first hydration shell involve in-plane waters bridging pairs of nitrate oxygens with two equal and bent hydrogen bonds. A second extremely labile local minimum involves out-of-plane waters with a single hydrogen bond and lies about 2 kcal/mol higher. The potential in the region of the second minimum is extremely flat and qualitatively sensitive to changes in the basis set; it does not correspond to a true equilibrium structure.

1 Introduction

Nitrate ion hydration complexes play an important role in elementary mechanisms of cloud nucleation [1, 2], polar stratospheric cloud chemistry [3], D-region negative ion chemistry [5], and tropospheric NO_x and acid deposition chemistry. The structure and energetics of nitrate hydration clusters is therefore of environmental and aeronomic interest. Thermodynamic properties of hydrated nitrate anions have been investigated using high-pressure

¹Present Address: Dept. of Chemistry, Frostburg State University, Frostburg MD 21532

mass spectroscopy by Lee [6, 7], Payzant [8], and Fehsenfeld [5] and coworkers.

Lee and coworkers [7] performed CNDO/2 calculations on one, two, and three water nitrate anion hydrates. Their calculations showed bent hydrogen bonds with lengths of 1.38, 1.40, and 1.42 Å, respectively, with $\angle \text{H} - \text{O} - \text{N} = 115^\circ$. Configurations with water lying out of the plane of the anion were slightly favored over planar complexes. The first *ab initio* studies of nitrate anion hydration complexes were performed by Howell and coworkers [12]. Their study treated one-, two, and three-water complexes at the 6-31G/SCF level. Geometry optimizations were severely constrained, with only planar complexes with water fixed at its experimental equilibrium geometry being considered. Single hydrogen bonds were further constrained to be linear. The two and three-water complexes were restricted to a few high symmetries. No vibrational analyses were performed to verify that the geometries were true local minima. A recent SCF study by Shen, Xie, Schaefer, and Deakyne [13] reported completely optimized stationary points of the monohydrate potential surface using a double-zeta plus polarization basis set. Anion diffuse functions were not included in the basis since these functions have relatively little effect on computed binding energies; however it is generally accepted that diffuse functions are necessary to provide an adequate description of anionic charge densities [14] and hydrogen bonded complexes. A C_{2v} structure with two hydrogen bonds (with a binding energy of 14.9 kcal/mole) and a structure with a single hydrogen bond (with a binding energy of 12.3 kcal/mole) were reported. Both structures were planar. In a subsequent study of isomers of the conventional nitrate monohydrate complex [15], single-point calculations including anion diffuse functions were performed at geometries which were optimized without the benefit of this refinement.

In the present study, the dependence of the qualitative and quantitative aspects of the SCF potential energy surfaces of singly, doubly, and triply hydrated nitrate anions on the quality of the basis set has been investigated. Additionally, thermodynamic properties of $\text{NO}_3^-(\text{H}_2\text{O})_n$ complexes have been computed at the SCF level using a valence triple zeta quality basis set with both polarization and anion-diffuse functions. Geometry optimizations were completely unrestrained. Vibrational analyses using computed first and second energy derivatives were performed for each optimized geometry. Equilibrium concentration ratios of $\text{NO}_3^-(\text{H}_2\text{O})_n$ complexes under ionospheric and

polar stratospheric conditions are predicted using the *ab initio* thermochemical parameters with a standard atmosphere model.

2 Method

Ab initio self-consistent field calculations and vibrational analyses were performed on $\text{NO}_3^-(\text{H}_2\text{O})_n$ complexes (with $n = 1, 2$, and 3) using the GAMESS program [17]. Three basis sets were used:

- A Dunning/Hay double zeta plus polarization (DZP) basis set with scale factors of 1.2 and 1.15 for hydrogen [16, 17] was used for preliminary exploration of the potential energy surfaces. This N, O (10s5p1d)/[3s2p1d], H (4s1p)/[2s1p] basis set contains 85, 110, and 135 contracted Gaussian functions for $\text{NO}_3^-(\text{H}_2\text{O})_n$ calculations with $n = 1, 2$, and 3 , respectively.
- An extended Pople 6-311G** basis set[18] augmented with anion diffuse *sp* shells ($\zeta = 0.0845$)[19] centered on each nitrate oxygen was used to obtain fully optimized one- and two-water complex geometries. With this triple zeta plus polarization plus diffuse basis set (TZP+) there are 119, 150, and 181 contracted Gaussian functions for the singly, doubly, and triply hydrated complexes, respectively.
- An N, O (13s8p2d)/[7s4p2d], H (8s2p)/[5s2p] van Duijneveldt basis set [20, 21] augmented with anion diffuse *sp* shells ($\zeta = 0.06$) on the nitrate oxygens was used to compute $\text{NO}_3^-(\text{H}_2\text{O})$ complex binding energies and charge density maps at the TZP+ optimal geometries. This quadruple zeta plus double polarization plus anion diffuse (QZ2P+) basis set contains 189 contracted Gaussian functions for the monohydrate complex.

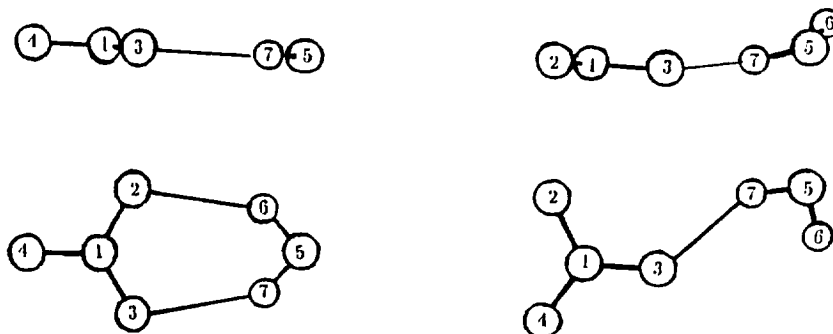
The accuracy of SCF level hydrogen bonding energies is limited by the ability of the basis set to describe the properties of the individual fragments. Errors in fragment dipole moments, static polarizabilities and ionization potentials will propagate to errors in the electrostatic, polarization, and charge-transfer contributions to the hydrogen bond energies, respectively. [22] Energies and structures computed for the isolated nitrate and water fragments are compared with those obtained by experiment and previous SCF calculations in Table 1.

Table 1: *Optimized geometries and properties of isolated H₂O and NO₃⁻ fragments. Distances are in Å, angles are in degrees, energies are in a. u., and dipole moments are in Debyes.*

Fragment	Source	Optimized Geometry		Total Energy	Dipole Moment
H ₂ O		R_{OH}	$\angle HOH$		
	1	0.940	106.4°	-76.06370	2.00
	2	0.941	106.9°	-76.060411	2.25
	3	0.941	104.4°	-76.04709	2.14
	4	0.941	107.1°	-76.05604	2.25
	6	0.944	106.7°	-76.04683	2.19
	7	0.95781	104.4776	...	1.8546
NO ₃ ⁻		R_{NO}			
	1	1.222		-279.04831	0.0
	2	1.224		-279.03967	0.0
	3	1.222		-279.01063	0.0
	4	1.223		-279.02533	0.0
	5	1.26		-278.7676	0.0
	6	1.231		-278.99006	0.0

1. This work; SCF with QZ2P+ basis.
2. This work; SCF with a basis that is the same as the QZ2P+ basis but with only one *d* polarization function on O, N and only one *p* polarization function on H.
3. This work; SCF with TZP+ basis. The SCF/TZP+ vertical ionization potentials for water and nitrate anion are 0.4011 and 0.1645 hartrees, respectively.
4. This work; SCF with a Dunning triple split valence [23] plus polarization plus anion diffuse *sp* shells on nitrate oxygens.
5. See Reference [12]. SCF with Pople 6-31G basis set.
6. This work; SCF with DZP basis. The SCF/DZP ionization potentials for water and nitrate anion are 0.4023 and 0.1590, respectively.
7. Experimental values; see References [25] and [26] for water.

Figure 1: Optimized geometries, total energies and dipole moments of mono-hydrate complexes of NO_3^- .



Structure	Ia	Ib
E_{total} (a. u.) (DZP)	-355.061144	-355.056901
(TZP+)	-355.080509	-355.077085
(QZ2P+)	-355.133512	
μ_D (Debye) (DZP)	0.140	1.927
(TZP+)	0.452	1.801
(QZ2P+)	0.368	

The TZP+ energy and dipole moment of water is only a slight improvement over that of the DZP basis but is significantly better than that provided by the 6-31G basis. The SCF/QZ2P+ basis yields a total energy for water that estimated to be 0.0038 a. u. above the SCF limit [24] and overestimates the gas phase dipole moment of water by only 8%.

3 Results and Discussion

Optimized geometries of the mono, di, and trihydrate complexes are shown in Figures 1, 2, and 3, with a comparison of geometric parameters shown in Table 2.

The most stable geometries in the first hydration shell involve in-plane waters bridging pairs of nitrate oxygens with two equal and bent hydrogen

Figure 2: Optimized geometries, total energies and dipole moments of dihydrate complexes of NO_3^- .

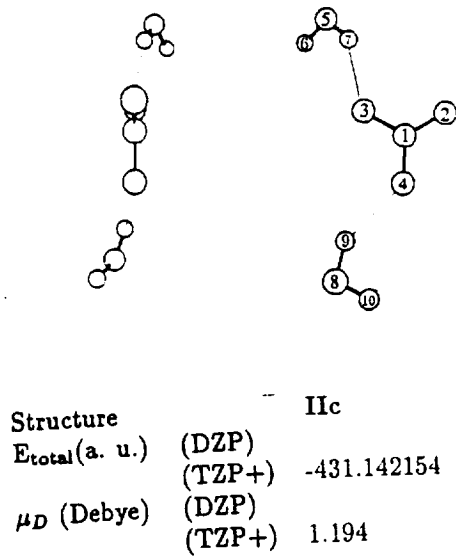
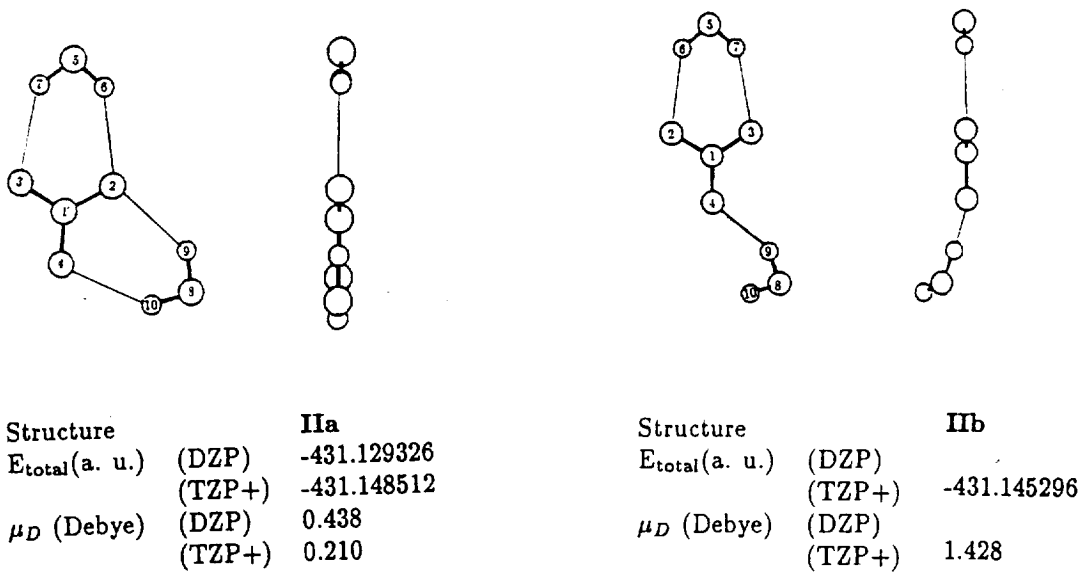
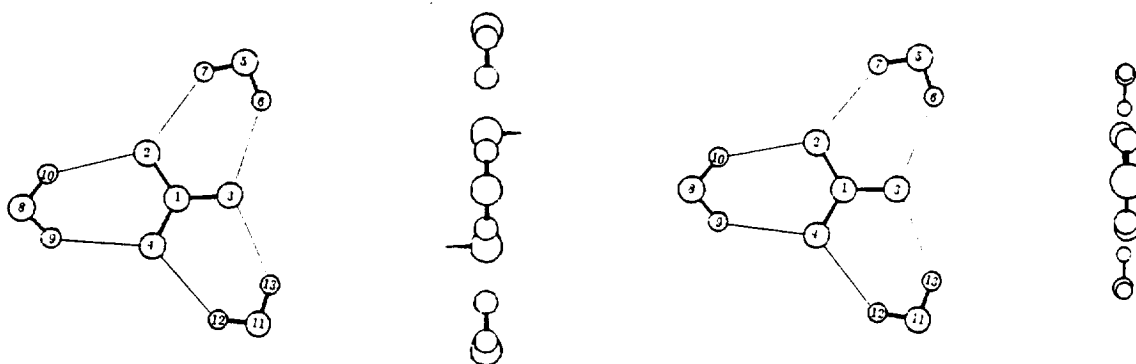


Figure 3: Optimized geometry of the most stable trihydrate of NO_3^- . The D_{3h} geometry **IIIa** is a local minimum in the DZP basis and a double saddle point in the TZP+ basis. The arrows on the in-plane view show nuclear displacement vectors corresponding to one of the TZP+ doubly degenerate imaginary frequencies. **IIIb** is the local minimum in the TZP+ basis.



Structure		IIIa	IIIb
E_{total} (a. u.)	(DZP)	-507.195071	
	(TZP+)	-507.214732	(TZP+) -507.214736
μ_D (Debye)	(DZP)	0.00	
	(TZP+)	0.00	(TZP+) 0.03

bonds. A second energy minimum involves out-of-plane waters with a single strong hydrogen bond and lies about 2 kcal/mol higher. Computed total energies and thermochemical properties of the hydration complexes (and fragments) are given in Table 4. The thermochemical properties were computed using the ideal gas, rigid rotor, and harmonic normal mode approximations at standard temperature and pressure. The larger dipole moment predicted by the DZP basis in conjunction with greater basis set superposition error leads to slightly higher binding energy estimates than those obtained with the more extensive bases.

The $\text{NO}_3^- \cdots \text{H}_2\text{O}$ Potential

The C_{2v} local minimum at **Ia** closely resembles the doubly hydrogen bonded monohydrate structures reported by Howell *et. al.* and Shen *et. al.* The pair of symmetric bent hydrogen bonds at the SCF/TZP+ level are 0.02 Å longer and about 0.5° more bent than those computed by the latter authors with a double zeta plus polarization basis set.

Figure 4 shows slices through the potential well at **Ia** at a) fixed nitrate oxygen to water oxygen distances R_{OO} and b) at fixed water roll angle θ about its dipole. The shape of the roll angle curve can be qualitatively explained using a simple point charge model; the planar configuration is electrostatically favored.

Figure 6 shows the effect of complex formation on the QZ2P+ charge density distribution for structure **Ia**. Polarization of the water is the primary effect of complexation on the charge density. Figure 5 shows the effect of complex formation on the orbitals of the nitrate and water fragments at the QZ2P+ level; the electron donor orbitals are lowered and the proton donor orbitals are raised [22].

A second TZP+ local minimum (**Ib**) involves out-of-plane waters with a single strong hydrogen bond and lies about 2 kcal/mol higher than structure **Ia**. The potential in the region of **Ib** is extremely flat and quite sensitive to basis set changes; for example, in the DZP basis **Ib** collapses to a planar structure. Two saddle points were located in this region on the TZP+ surface:

1. **Ic** has C_s symmetry lies at -355.076978 and resembles equilibrium geometries reported by Lee *et. al.* and Shen *et. al.* at the CNDO and double zeta plus polarization level, respectively. However, at the SCF/TZP+ level this structure is a saddle point. The single imaginary

Table 2: $\text{NO}_3^- \cdots \text{H}_2\text{O}$ complex stationary point geometries. Distances are in Å, angles are in degrees.

Structure	Basis	R_{12}	R_{13}	R_{14}	R_{26}	R_{37}	R_{56}	R_{57}
Ia	DZP	1.235	1.235	1.222	2.185	2.185	0.949	0.949
	TZP+	1.226	1.226	1.213	2.209	2.209	0.946	0.946
Ib	DZP	1.227	1.240	1.224	4.227	2.006	0.943	0.956
	TZP+	1.217	1.231	1.215	4.383	1.987	0.941	0.951
IIa	DZP	1.239	1.226	1.226	2.209	2.238	0.949	0.948
	TZP+	1.230	1.217	1.217	2.216	2.253	0.945	0.945
IIb	TZP+	1.221	1.219	1.222	2.241	2.225	0.945	0.945
IIc	TZP+	1.211	1.224	1.226	4.840	2.012	0.941	0.950
IIIa	DZP	1.230	1.230	1.230	2.258	2.258	0.948	0.948
IIIb	TZP+	1.221	1.221	1.221	2.253	2.265	0.945	0.944

Structure	Basis	$\angle 213$	$\angle 214$	$\angle 126$	$\angle 137$	$\angle 265$	$\angle 375$	$\angle 657$
Ia	DZP	119.9	120.2	111.2	111.2	139.2	139.2	99.6
	TZP+	119.5	120.3	111.5	111.5	138.9	138.9	99.7
Ib	DZP	119.4	120.8		115.2		149.3	103.0
	TZP+	119.7	119.6		130.9		147.6	102.0
IIa	DZP	119.8	119.8	110.9	111.9	140.1	100.4	
	TZP+	119.7	119.7	111.0	112.0	140.4	100.2	
IIb	TZP+	120.2	119.9	111.1	111.6	138.2	100.2	
IIc	TZP+	120.3	120.3		134.8		102.2	
IIIa	DZP	120.0	120.0					
IIIb	TZP+	120.0	120.0	111.5	111.5	138.4	137.6	100.6

Structure	Basis	$\angle 1375$	$\angle 4137$	$\angle 2149$	$\angle 1498$	$\angle 498$	10
Ib	DZP	0.0	180.0				
	TZP+	144.8	166.5				
IIb	TZP+	-0.7	-179.6	13.5	143.9	-12.4	
IIc	TZP+	-151.3	-12.2	11.0	151.0	-10.6	

Structure	Basis	R_{49}	R_{98}	$R_{8\ 10}$	$\angle 149$	$\angle 498$	$\angle 9\ 8\ 10$
IIb	TZP+	2.019	0.950	0.941	130.2	146.6	102.2
IIc	TZP+	2.015	0.950	0.941	132.3	146.9	102.3

frequency leads to equivalent structures **Ib** above and below the plane of the nitrate ion through torsion around the hydrogen bond and the adjacent nitrate NO and water OH bonds. **Ic** lies only 0.07 kcal above **Ib** so the motion of water between the equivalent **Ib** structures through the anion plane is barrier free.

2. Structure **Id** is a saddle point along the minimum-energy path between structures **Ia** and **Ib** and lies at -355.077059 hartrees; conversion of **Ib** to **Ia** is therefore also barrier free.

Figure 7 shows a slice through the potential energy surface corresponding to torsion about the hydrogen bond to show the relationship between the minima at **Ia** and **Ib** and the saddlepoint **Id**. The flatness of the potential in the region around **Ib** precludes its consideration as an equilibrium "structure". Note that the minimum **Ib** has a D_e of 12.5, 12.1, and 11.3 kcal/mol at the SCF/DZP, SCF/TZP+, and SCF/QZ2P+ levels, respectively; Shen's singly hydrogen bonded structure has a D_e of 12.3 kcal/mol [13].

Several higher order stationary points were located. A planar C_{2v} structure with two "bifurcated" hydrogen bonds involving a single nitrate oxygen lies at -355.076019 hartrees. A second C_{2v} structure with water lying in the anion's σ_v plane and bisecting the O-N-O angle lies at -355.075744 hartrees. Both structures are double saddle points.

Table 3 lists vibrational frequencies and infrared intensities computed at the TZP+/SCF level for complexes **Ia**, **IIa**, and **IIIb**. The solvated nitrate ion in dilute alkali metal nitrate solutions gives rise to observed frequencies at 1404 cm^{-1} , 1348 cm^{-1} , 1049 cm^{-1} , 825 cm^{-1} , and 719 cm^{-1} [32]. Note that energy first and second derivatives are consistently overestimated at this level of theory [27]; a scaling factor of 0.89 is often applied to calculated frequencies in comparisons with experimental spectra. While the anharmonicity of the potential surface and inherent deficiencies at the SCF level of theory preclude quantitative prediction of spectroscopic observables, the calculations qualitatively predict many features of aqueous alkali metal nitrate Raman and infrared spectra.

The experimentally observed splitting of the $\nu_3(E')$ nitrate band in solution has been attributed to lowering of the anion symmetry by the ion-water interaction [32]; our calculations support this interpretation. The experimental splitting for dilute aqueous alkali metal nitrates is 56 cm^{-1} ; the calculated

Figure 4: Lability characteristics of water in the C_{2v} doubly hydrogen bonded $\text{NO}_3^-(\text{H}_2\text{O})$ complex **Ia**. R is the distance (in angstroms) from the nitrate nitrogen to the water oxygen; θ_2 is the water roll angle about C_2 axis.

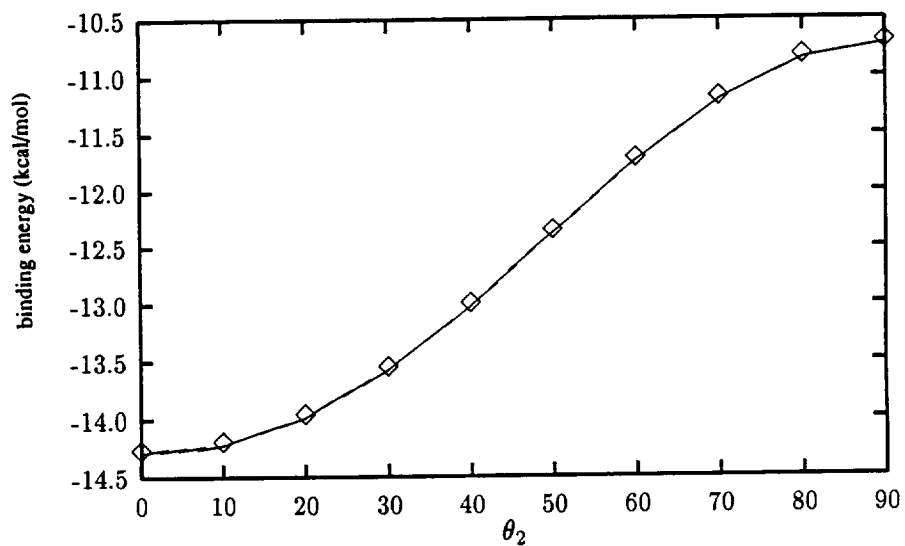
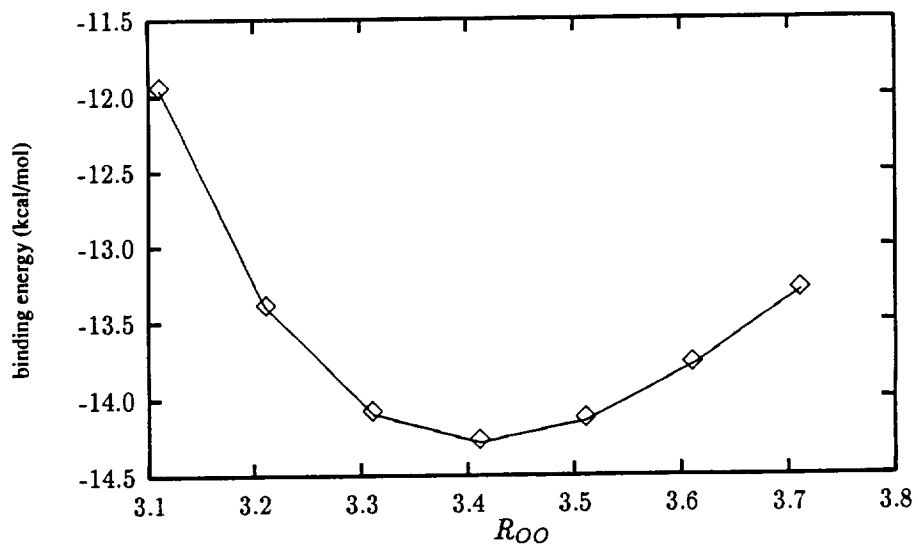
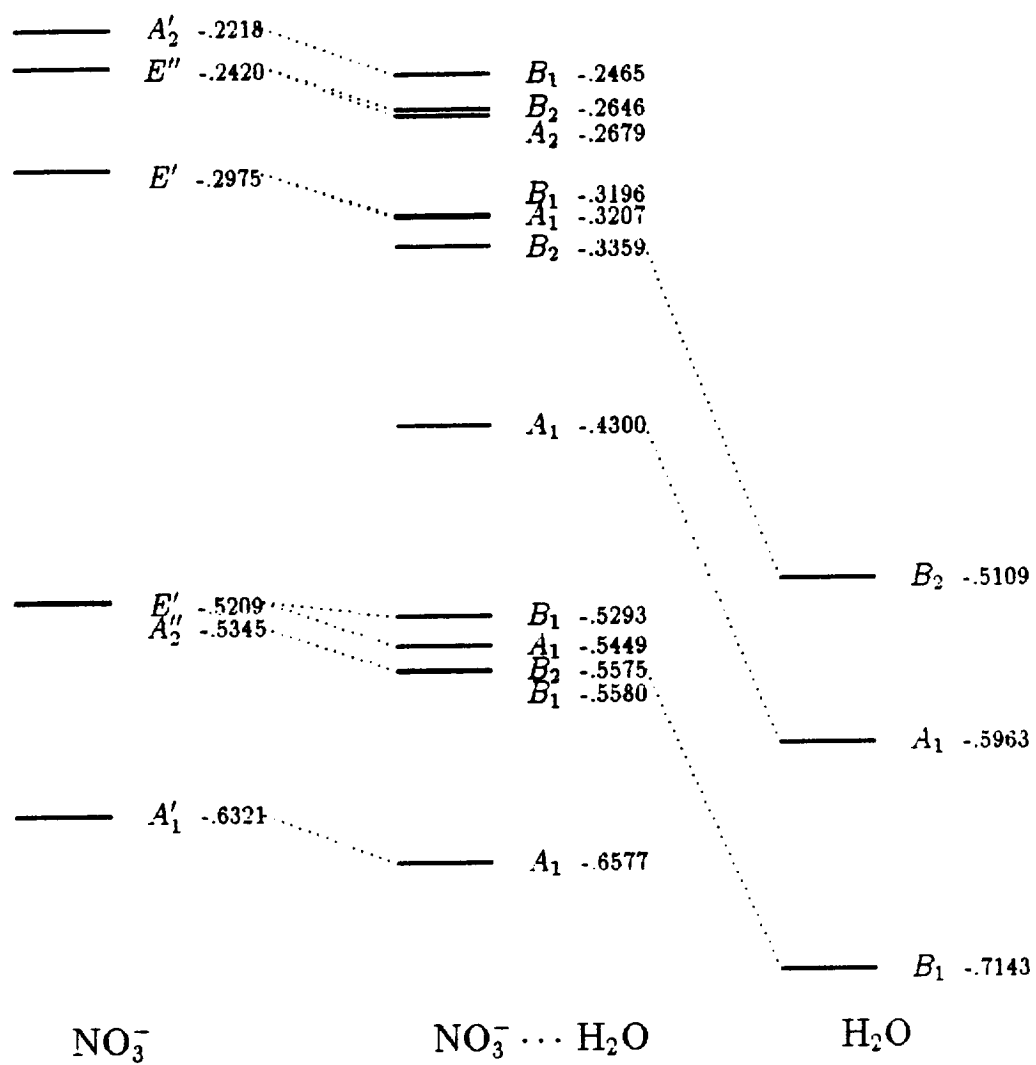


Figure 5: $QZ2P+$ molecular orbital energies for complex Ia.

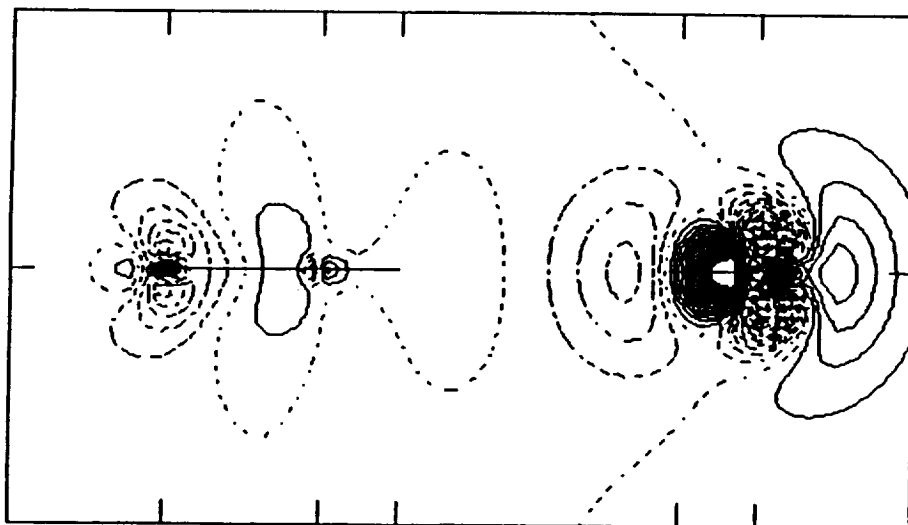


Figure 6: $QZ2P+$ charge density difference plot for Ia obtained by subtracting the isolated fragment one-electron densities from those of the complex. The solid lines are contours of increased charge density due to complex formation, while the broken lines represent lowered density contours.

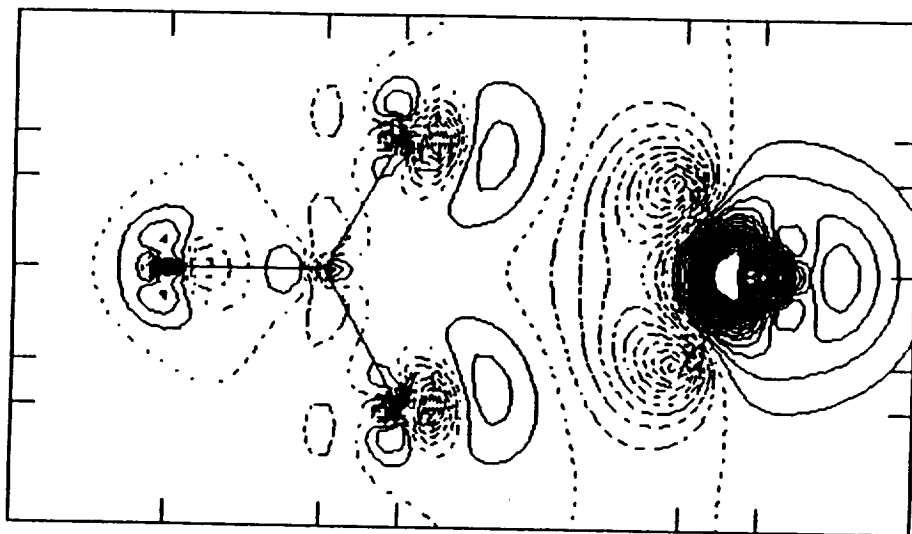
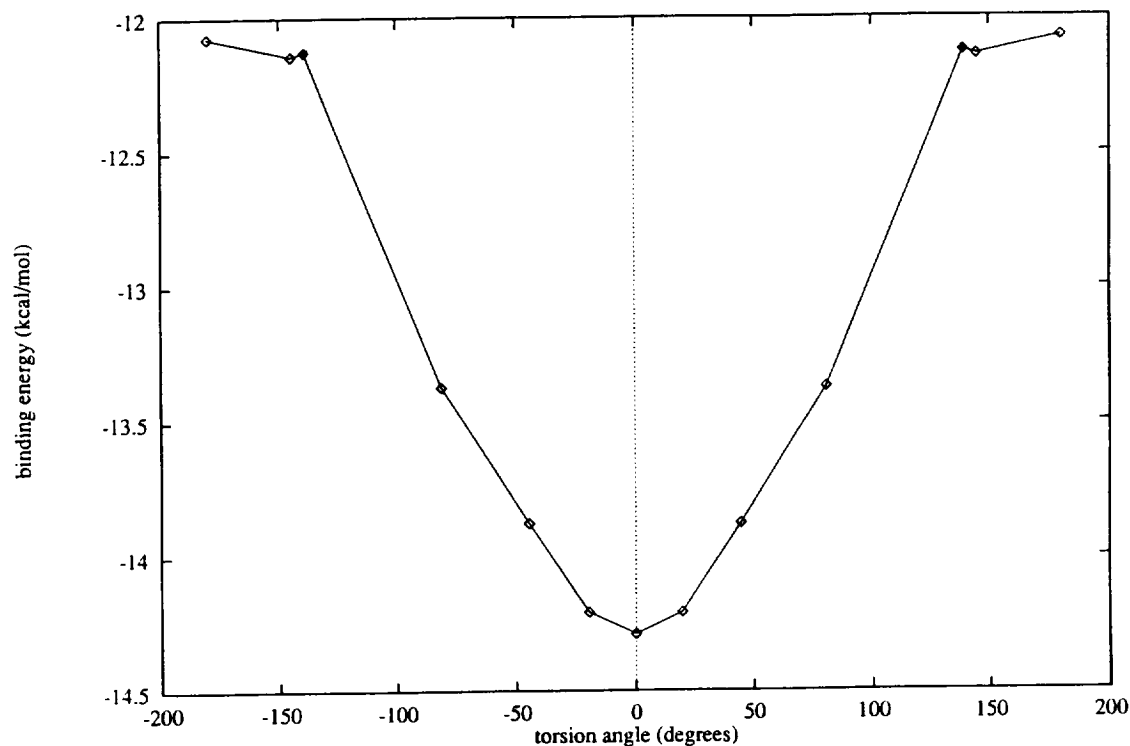


Figure 7: Monohydrate hydrogen bond torsion potential. Geometries with the hydrogen bond torsion angle fixed at the indicated angle with all other geometric parameters optimized are marked by diamonds. The solid diamond indicates the position of the saddle point Id.



splitting is 39 cm^{-1} for the monohydrate **Ia** and 38 cm^{-1} for the dihydrate **IIa**. However splitting of the $\nu_4(E')$ band due to solvent water is predicted to be very small (being less than one wavenumber for **Ia** and less than 5 wavenumbers for **IIa**). This is in accord with Irish's observation that $\nu_4(E')$ splittings occur only in concentrated solution and appear to indicate proximity of the cation [33].

The lowest 6, 13, and 18 frequencies in the spectra of complexes **Ia**, **IIa**, and **IIIb**, respectively, are associated with rather facile motions about hydrogen bond.

Multiple Hydration Complexes

Table 3: *Computed vibrational spectra for complexes Ia, IIa, IIIa and infinitely separated water and nitrate fragments. Frequencies are in reciprocal centimeters; infrared intensities are in Debye²/amu-Å².*

Ia		IIa		IIIa		NO ₃ ⁻ + H ₂ O		
Freq.	Int.	Freq.	Int.	Freq.	Int.	Freq.	Int.	
804	0.0	805	0.0	811	0.03	799	0.0	NO ₃ ⁻ ν ₄ (E')
804	0.0	810	0.0	811	0.03	799	0.0	NO ₃ ⁻ ν ₄ (E')
977	1.0	974	1.1	973	1.2	980	0.8	NO ₃ ⁻ ν ₂ (A ₂ '')
1234	0.1	1234	0.1	1239	0.0	1234	0.0	NO ₃ ⁻ ν ₁ (A ₁ ')
1552	17.8	1560	18.1	1578	23.0	1570	21.0	NO ₃ ⁻ ν ₃ (E')
1596	25.6	1598	26.7	1578	23.0	1570	21.0	NO ₃ ⁻ ν ₃ (E')
1839	3.2	1829	4.2	1823	4.8	1750	1.9	H ₂ O bend
		1840	2.1	1823	4.9			
				1837	0.0			
4109	3.2	4102	3.0	4124	4.0	4141	0.4	H ₂ O sym. stretch
		4145	2.8	4124	4.0			
				4126	0.01			
4139	1.8	4157	1.7	4165	0.006	4236	1.3	H ₂ O asym. stretch
		4182	1.8	4168	2.5			
				4168	2.5			

1. Hydrogen bond vibrational frequencies (and intensities) for structure Ia are 32 cm⁻¹ (0.0), 87 cm⁻¹ (0.5), 165 cm⁻¹ (0.2), 227 cm⁻¹ (2.3), 235 cm⁻¹ (0.0), and 648 cm⁻¹ (5.9).
2. Hydrogen bond vibrational frequencies (and intensities) for structure IIa are 22 cm⁻¹ (0.02), 34 cm⁻¹ (0.0), 45 cm⁻¹ (0.3), 108 cm⁻¹ (0.4), 150 cm⁻¹ (0.01), 165 cm⁻¹ (0.2), 185 cm⁻¹ (0.01), 193 cm⁻¹ (0.001), 213 cm⁻¹ (2.4), 266 cm⁻¹ (2.6), 604 cm⁻¹ (0.04), and 613 cm⁻¹ (11.6).
3. Hydrogen bond vibrational frequencies (and intensities) for structure IIIa are: 9 cm⁻¹ (0.01), 19 cm⁻¹ (0.04), 29 cm⁻¹ (0.02), 46 cm⁻¹ (0.3), 47 cm⁻¹ (0.3), 83 cm⁻¹ (0.0001), 127 cm⁻¹ (0.002), 135 cm⁻¹ (0.0003), 144 cm⁻¹ (0.2), 150 cm⁻¹ (0.002), 156 cm⁻¹ (0.05), 158 cm⁻¹ (0.002), 189 cm⁻¹ (3.9), 193 cm⁻¹ (3.9), 217 cm⁻¹ (0.003), 569 cm⁻¹ (0.02), 569 cm⁻¹ (0.04), 587 cm⁻¹ (17.3)

In structure **IIa** the water-water interaction is about +1.2 kcal/mole at the TZP+/SCF level (assuming that fragment interactions are pairwise additive.). The net repulsive interaction leads to slightly weaker hydrogen bonds but both waters remain in the plane and the angle between water oxygens (with vertex at the nitrate nitrogen) does not open significantly (119.7°). Induction associated with geminal hydrogen bonding drives Mulliken and Löwdin charges on the doubly hydrogen bound nitrate oxygen 12% and 15% higher than those on the singly hydrogen-bound nitrate oxygens, but geminal hydrogen bonds are still 0.03 – 0.04 Å longer than nongeminal bonds.

Stationary points at **IIb** and **IIc** involve one and two waters, respectively, in highly labile singly hydrogen bonded sites. Again, the potential around these sites is extremely flat and **IIb** and **IIc** are not well-defined equilibrium structures despite the fact that they are mathematical minima. At the SCF/TZP+ level, D_e is 25.4 and 23.4 kcal/mol for **IIb** and **IIa**, respectively. The repulsive interaction between singly and doubly waters in structure **IIb** hydrogen bound sites is about 1.0 kcal/mol, while repulsion between pairs of singly bound waters on opposite sides of the anion plane is 0.8 kcal/mol.

The most stable SCF/DZP trihydrate complex **IIIa** has D_{3h} symmetry. However, a D_{3h} optimization at the SCF/TZP+ level yields a double saddle point at -507.214732 hartrees. The degenerate imaginary vibrational frequencies lead to a minimum energy structure with a slight out-of-plane distortion of the complex (see Figure 3). The minimum energy structure lies only four microhartrees below the planar double saddle point structure. If pairwise ion-water and water-water interactions are additive, D_e for the three-water complex **IIIa** is expected to be $3*14.3 - 3*1.2 = 39.3$ kcal/mol. The complex is very slightly more bound than this ($D_e = 39.4$ kcal/mol).

Atmospheric Implications

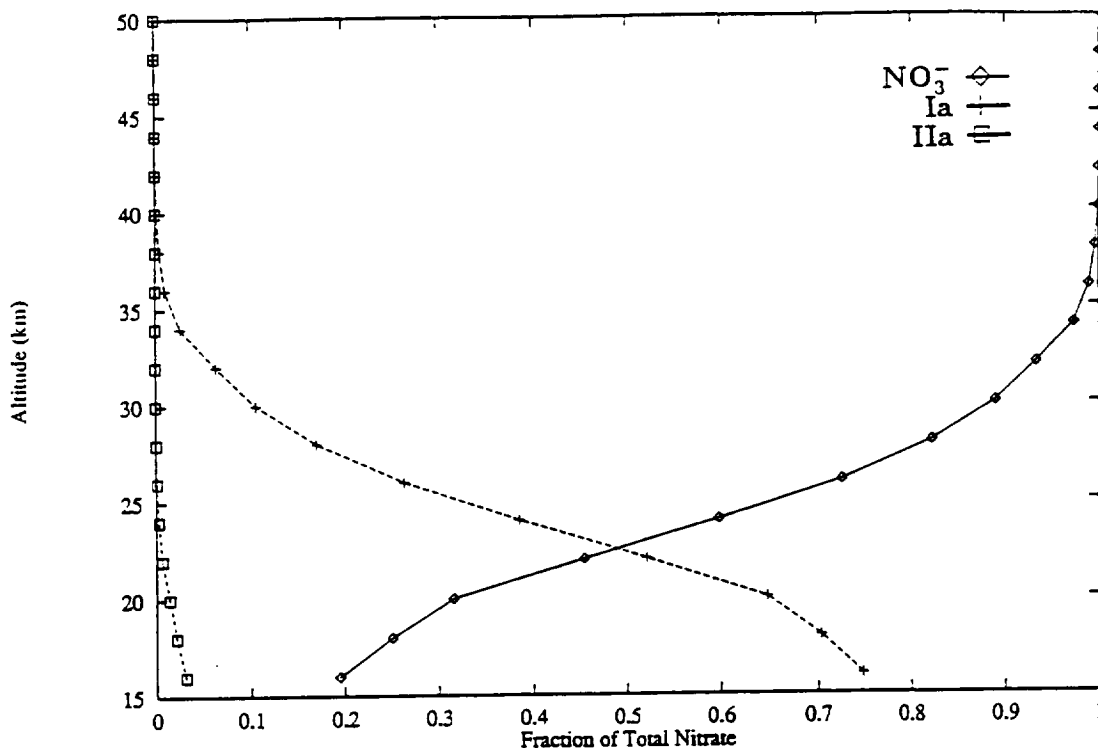
Figure 8 gives the altitude profile of the mono- and dihydrate complexes as fractions of total nitrate considering only NO_3^- and H_2O in equilibrium, using a constant water concentration of 5 ppm by mass and the 1976 Standard Atmosphere temperature and density profiles [35]. While quantitative predictions require consideration of other species (particularly HNO_3), concentrations of di- and trihydrate complexes in the stratosphere and lower mesosphere under these conditions are predicted to be very low.

Table 4: Theoretical versus experimental thermochemical quantities for the clustering of n water molecules on NO_3^- .

n	D_e	D_0	$\Delta H_{0,n}^0$	$\Delta S_{0,n}^0$	Method	Source
1 (Ia)	15.2 ¹	13.1	-13.4	-25.0	SCF/DZP	This work
	14.3	12.3	-12.6	-21.7	SCF/TZP+	This work
	13.5				SCF/QZ2P+	This work
	18.5				SCF/6-31G	Ref. [12]
	14.9	12.8			SCF/DZP	Ref. [13]
	(exper.)			-12.4	-19.1	HP MS
			-14.6	-25.0	HP MS	Ref. [6]
2 (IIa)	28.6	24.6	-25.1	-49.0	SCF/DZP	This work
	27.4	23.6	-24.0	-45.4	SCF/TZP+	This work
	35.2				SCF/6-31G	Ref. [12]
	(exper.)			-28.9	-55.3	HP MS
3 (IIIa)	40.5	34.9	-35.3	-71.5	SCF/DZP	This work
	(exper.)			-42.7	-88.5	HP MS

1. The Boys counterpoise corrected values for D_e for monohydrate complex Ia are 14.7 and 13.1 kcal for the DZP and TZP+ bases, respectively.

Figure 8: Equilibrium distribution of nitrate hydrates in the stratosphere and lower ionosphere, assuming a water concentration of 5 ppm.



Equilibria under polar stratospheric conditions were modeled in the temperature range from 190°K to 200°K with an upper limit on the water concentration equal to the vapor pressure of ice. 57% to 54% of the total nitrate present exists as monohydrate Ia and 36% to 40% exists as dihydrate IIa (considering only nitrate and water in equilibrium). The trihydrate IIIa and dihydrate IIb each account for 2%. About 1% of total nitrate exists as the singly hydrogen bound monohydrate Ib and only 0.6% of total nitrate is predicted to exist in unhydrated form under these conditions.

4 Conclusions

Completely optimized equilibrium geometries, vibrational frequencies, thermochemical parameters, and stable site labilities of nitrate ion hydration complexes involving 1, 2, and 3 waters have been presented. The most stable geometries in the first hydration shell involve in-plane waters bridging pairs of nitrate oxygens with two equal and bent hydrogen bonds. A second extremely labile local minimum involves out-of-plane waters with a single hydrogen bond and lies about 2 kcal/mol higher.

The potential in the region of the second minimum is extremely flat and qualitatively sensitive to changes in the basis set; it does not correspond to a true equilibrium structure. A small but qualitative change in the geometry of the minimum energy trihydrate structure occurs in moving from the DZP to the TZP+ basis. Our results emphasize that the positions of mathematical minima on the energy hypersurfaces provide an incomplete description of the structure of weakly bound complexes. The potential around the minimum must be explored to characterize the lability of the complex, and this exploration should employ several different basis sets in order to detect basis set artifacts.

Acknowledgement

This work has been supported by a cooperative agreement with the Old Dominion Research Foundation under contract NCCI147.

References

- [1] B. D. Kay, V. Hermann, A. W. Castleman, *Chem. Phys. Letters*, **80**, 469 (1981).
- [2] A. W. Castleman Jr., *Adv. Colloid Interface Sci.*, **10** 73 (1979).
- [3] R. T. Watson, M. J. Kurylo, M. J. Prather, F. M. Ormond, "Present State of Knowledge of the Upper Atmosphere 1990: An Assessment Report", NASA Reference Publication 1242, 1990.
- [4] P. J. Crutzen, F. Arnold, *Nature*, **324**, 651 (1976).
- [5] F. C. Fehsenfeld, E. F. Ferguson, *J. Chem. Phys.*, **61**, 3181 (1974).

- [6] N. Lee, R. G. Keese, A. W. Castleman. *J. Am. Chem. Soc.*, **101**,2599 (1979).
- [7] N. Lee, R. G. Keese, A. W. Castleman, Jr., *J. Chem. Phys.*, **72**, 1089 (1980).
- [8] J. D. Payzant, R. Yamdagni, P. Kebarle, *Can. J. Chem.*, **49**, 3308 (1971).
- [9] P. Noble, R. Kortzeborn, *J. Chem. Phys.*,**52**, 5375 (1970). C. F. Bender, C. W. Bauschlicher, H. F. Schaefer, *J. Chem. Phys.*, **60**, 3707 (1974)
- [10] P. Kebarle, Higher-order Reactions- Ion Clusters and Ion Solvation. in *Ion-Molecule Reactions*, J. L. Franklin ed., Butterworths, London, **1**, 315-362 (1971).
- [11] R. S. Narcisi, A. D. Bailey, L. Della Lucca, C. Sherman, D. M. Thomas, *J. Atmos. Terr. Phys.*,**33**,1147-1159 (1971).
- [12] J. M. Howell, A. M. Sapse, E. Singman, G. Snyder, *J. Phys. Chem.*, **86**, 2345 (1982).
- [13] M. Shen, Y. Xie, H. F. Schaefer III, C. A. Deakyne, *J. Chem. Phys.*, **93**, 3379 (1990).
- [14] J. Simons, *Int. J. Quant. Chem.*, **11**, 971 (1977).
- [15] M. Shen, Y. Xie, H. F. Schaefer III, C. A. Deakyne. *Chem. Phys.*,**151**, 187 (1991).
- [16] T. H. Dunning, Jr., P. J. Hay, in *Methods of Electronic Structure Theory*, H. F. Schaefer III, Ed., Plenum Press, N. Y. (1977), pp 1-27.
- [17] M. W. Schmidt, K. K. Baldridge, J. A. Boatz, J. H. Jensen, S. Koseki, M. S. Gordon, K. A. Nguyen, T. L. Windus, S. T. Elbert, *QCPE Bulletin*, **10**, 52-54 (1990).
- [18] R. Krishnan, J. S. Binkley, R. Seeger, J. A. Pople. *J. Chem. Phys.*, **72**, 650-654 (1980).
- [19] T. Clark, J. Chandrasekhar, G. W. Spitznagel, P. von R. Schleyer, *J. Comput. Chem.*, **4**, 294-301 (1983).
- [20] F. B. van Duijneveldt, *IBM Res. J.* , **945** (#16437), (1971).
- [21] G. L. Lie, E. Clementi, *J. Chem. Phys.*, **60**, 1275 (1974).

- [22] P. A. Kollman. Hydrogen Bonding and Donor-Acceptor Interactions. in *Modern Theoretical Chemistry 4: Applications of Electronic Structure Theory*, (H. F. Schaefer III ed.), Plenum Press, pp 109-144 (1977).
- [23] T. H. Dunning, *J. Chem. Phys.*, **55** 716-723 (1971).
- [24] F. F. Roelandt, D. F. van de Vondel, G. P. van der Kelen, *J. Mol. Struct.*, **54**, 221 (1979).
- [25] A. R. Hoy, I. M. Mills, G. Strey, *Mol. Phys.*, **24**, 1265 (1972).
- [26] A. R. Hoy, P. R. Bunker, *J. Mol. Spectrosc.*, **74**, 1 (1979).
- [27] L. J. Schaad, Theory of the Hydrogen Bond, in *Hydrogen Bonding*, M. D. Joesten and L. J. Schaad, eds.), Marcell Dekker, Inc., New York (1974), chapter 2.
- [28] A. Banerjee, J. Simons, *J. Chem. Phys.*, **71**, 60 (1979).
- [29] A. Banerjee, R. Shepard, J. Simons, *J. Chem. Phys.*, **73**, 1814-1826 (1980).
- [30] G. J. Janz, M. J. Tait, J. Meier, *J. Phys. Chem.*, **71**, 963 (1967).
- [31] C. B. Baddiel, M. J. Tait, G. J. Janz, *J. Phys. Chem.*, **69**, 3634 (1965).
- [32] D. E. Irish, A. R. Davies, R. A. Plane, *J. Chem. Phys.*, **50**, 2262 (1969).
- [33] D. E. Irish, A. R. Davies, *Can. J. Chem.*, **46**, 943 (1968).
- [34] H. Lee, J. K. Wilmshurst, *Australian J. Chem.*, **17**, 943 (1964).
- [35] *U. S. Standard Atmosphere, 1976*, NOAA, NASA, USAF, U. S. Government Printing Office, Washington D. C. (1976)